Egyptian Journal of Chemistry

http://ejchem.journals.ekb.eg/

Sounchemical synthesis of Graphene/nano hydroxyapatite composites for potential biomedical application

Ahmed M Bakr [a] *, Badawi Anis [a,b], Walid El hotaby [a]

[a] *Spectroscopy Department, Physics Division, National Research Centre, 33 El Bohouth st., Dokki, Giza, 12622, Egypt*
[b] *Molecular and Fluorescence Lab., Central Laboratories Network, National Research Centre, 33 El Bohouth Str., Dokki, 12622 Giza, Egypt*

Abstract

Graphene nanocrystalline hydroxyapatite composites (G/nHA) were prepared using a wet precipitation method with $CaCl_2$ and $Na_2 HPO_4$ as the main material in the presence of ultrasonic irradiation. The calcium to phosphate ratio (Ca/P) was adjusted to be about 1.67 while the pH value kept at 9.5-10.5. The texture properties of the G/nHA composites were determined through series of characterization techniques. High-resolution Scanning Electron Microscopy (HR-SEM) and high-resolution Transmission electron microscope (HR-TEM) were employed to determine the particle size and structure morphology of composites. The Crystalline and molecular structure were checked using (XRD), Raman and (FTIR), while thermal decomposition behavior was reported by thermogravimetric analysis (TGA-DTA). Energy dispersive spectroscopy (EDAX) results revealed that the prepared nHA and G2nHA samples had a Ca/P ratio of 1.66 and 1.73 respectively which are nearly matching to previously reported value. FT-IR analysis identified functional groups and confirmed the results obtained from the X-ray diffraction data that the prepared powders were indeed composed of nanoscale hydroxyapatite. The results indicate that nHA successfully prepared through this method and the range of particles was found around nanoscale. The compression test indicates that even the addition of very small amount of Graphene sheets like structure into the crystalline matrix of nHA enhancing the mechanical properties of the prepared composites compared to the pure nHA.

Keywords: Nanocrystal, hydroxyapatite, Graphene, structural characterization, mechanical evaluation, Biomaterials, Ultrasound.

1. Introduction

For a long time the efficient repair of hard tissues still a basic challenging target in the biomedical engineering science. Bioactive glasses, calcium phosphates, alumina, and zirconia, as assortment of biocompatible ceramics, have been utilized for many years in regenerative and reconstructive hard tissue procedures at uneven degrees of success. [1–6]. Completely biocompatible agent significantly must be considered for any ceramic being employed for a biomedical application. Additionally, it have be nontoxic, biologically stable, and non-immunogenic for biological tissues [7–9]. Therefore, calcium phosphates have been employed in bone replacement therapies, as it has the similar composition structure to the mineral phase found in bone [6,7]. Generally,

calcium phosphates are considers chemical stable, lightweight and commonly has the ions structure that established in the physiological environment besides its being compositionally similar [8]. Hydroxyapatite HA [$Ca_{10}(OH)_2 (PO_4)_6$,] and tri-calcium phosphate [$Ca_3(PO_4)_2$, TCP] are the main employed forms of the calcium phosphates in the biomedical applications field. Previous reports have indicated that HA has bioactivity and good biocompatibility and offers good osteoconductivity and osteoinductivity capabilities when it employed for bone tissue engineering applications [9][10][11][12]. In addition HA shows slow biodegradability besides it is the most thermodynamically stable calcium phosphate in physiological environment which provides tissue regeneration and tissue replacement to take place [11-15]. Due to its potential role in new bone tissue

_____

regeneration research, promote supplementary studies for its positive usage and elevates several processing techniques to synthesize it [16 -19]. Nevertheless, more efficient synthesis mechanism are currently developed to provided potential and massive quantities of HA nanopowders for future its usage in biomedical applications [19–22].

Recent studies and new research in nanoscience and nanotechnology have encouraged the researchers to through more light on the formation and investigation of HA in the Nano size scale and state obviously the new properties of HA at the nanoscale. There is a well-known fact about the field of nanotechnology stated that mostly all the physicochemical properties of the materials prepared at the nanoscale with different forms are altered compared with bulk size [21][20][21][22]. Based on lots of occasion, nanostructures of HA provided an excellent improvement of its properties.

Among various methods for HA nanocrystalline preparation, the wet chemical method is the most efficient method due to its low cost and simplicity, the precipitation method is considered a commonly wet chemical method used in calcium phosphate derivatives preparation. The chemical, physical and biological properties of the prepared nHA are influenced by various preparation parameters like preparation procedure, Ca/P ratio, pH value, particle size, and preparation temperature.

The well-known advantage of ultrasonic is producing superfine size slurries in addition, increase the speed of reaction, reaction output, and more efficacy energy usage. Furthermore, ultrasonic provides a valuable aid in the preparation process, gives more dispersion, and finally prevent the agglomeration of the prepared particles. Despite the excellent biocompatibility, the applications of pure HA in bone replacement material have been limited due to its low fracture stiffness, fragile nature, the inherent shaping difficulty and other short comings of porous HA in the load-bearing situations. A well-established method to enhanced the mechanical properties of HA scaffold is the improvement of HA matrix composite with different organic or inorganic materials [23]. Among those materials, the carbonaceous materials with high mechanical and chemical inertness are broadly recognized to exhibit good biocompatibility. Recently, with the growing development of graphene and regarding to its large surface area, low biological toxicity and good osteoinductive ability, it has been introduced into the field of tissue engineering [24]. Graphene derivatives like Graphene Oxide (GO) and reduced Graphene can be used as nano-filler materials in order to increase the mechanical property, osteogenesis, and biocompatibility of calcium phosphate and hydroxyapatite (HA) nanoparticles.

Therefore, in the present study, pure nano-hydroxyapatite (nHA) was synthesized using the wet precipitation method coupled with ultrasonic irradiation. In order to enhance the mechanical properties of the prepared nHA, Graphene sheets like structure are introduced into the nHA crystalline matrix with three loading percentages (G1nHA, G2nHA, and G3nHA). Then study the molecular structure of the prepared pure nHA and G/nHA composite and finally, evaluate the mechanical strength of the prepared samples.

2. Experimental

2.1. Materials

The chemicals used in this work include $CaCl_2$, Na_2HPO_4 and NaOH which were used as Ca^{2+}, PO_4^{3-}, and OH- sources respectively. The ultrasonic processor was an UP50H (50 W, 30 kHz) supplied by Hielscher ultrasound technology. All the reagents were analytical grade or highest purity available, and used without further purification. Aqueous solutions were prepared by dissolving the chemicals in Millipore deionized water.

2.2. Preparation of Graphene

First expandable graphite flakes (Asbury Carbons, USA, 3772, 300 mm nominal size) were thermally treated at 1050 C^0 for 15 s in argon atmosphere. Graphene dispersions were prepared through sonication of the expanded graphite powder (EG) in an aqueous of Pluronic (P-123) surfactant, as described previously by Guardia et al [25]. The initial concentration of the EG was 100 mg/mL and the surfactant concentration was adjusted to 1.0 wt%. The sonication time was continued for 2 h. To ensure the homogenization of the graphite powder, the graphite solution was stirred for 2 min each 30 min of

_____

sonication. Then the solution was centrifuged at 500 rpm for 1 h to remove unexfoliated graphite flakes. The top 65% supernatant was removed carefully and then subject to centrifugation at 20,000 rpm for 30 min to precipitate the exfoliated graphene sheets. The precipitated solid was washed several time with water to remove any surfactant may be present on the surface of the graphene layers. Then the sample was dried at 70oC under vacuum overnight.

2.3. Synthesis of Graphene nanohydroxyapatite

Graphene nanocrystalline Hydroxyapatite (GnHA) was fabricated as following, Firstly, 400 ml of 0.2 M of CaC_{l2} was treated with ultrasonic for 1h, then certain amount of graphene solution (0, 0.05, 0.1, 0.2 mg/ml) (pure nHA, G1nHA, G2nHA, G3nHA respectively) was treated previously with ultrasonic. Whilst under ultrasound irradiation, 400 ml of 0.12 M of Na_2HPO_4 was dropped using syringe pump (200 ml/h) under continuous ultrasonic irradiation (50 KW) and stirring, yielding a milky suspension. The pH value was checked and maintained at 9.5-10.5 at all times. A white precipitate was formed and the mixture was continuously irradiated with ultrasound for another 1h. The solution was filtered by centrifugation and washed two times with D.W, followed with ethanol and finally with D.I. then the white precipitates were dried for overnight at 100 °C. The samples were grained to fine powders and then transferred into ceramic boats and placed in an oven for thermal treatment at temperature of 600°C for 4h (10°C/min). Generally, the procedure is graphically presented as a flow chart in Figure 1.

2.4. Characterization

The obtained final products were grinded into fine powder and characterized using XRD, SEM and FT-IR spectroscopy. The structural characterization of the calcined nHA and GnHA nanopowders was identified by X- ray diffraction patterns were investigated by Broker D8 Advance, Germany X-ray diffraction (XRD) with CuKα 40kV/40mA and an incidence angle of 0.5° with wavelength equal to 1.5418 A°. The diffraction patterns were recorded automatically with a scanning rate of 2θ=2º/min. The samples were observed using a (JEM-1230FX, JEOLCo., Tokyo, Japan) operated at 120 kV. High

magnification (20K×, 150K×) brightfield (BF) images and selected are a diffraction (SAD) patterns were recorded using transmission electron microscope.
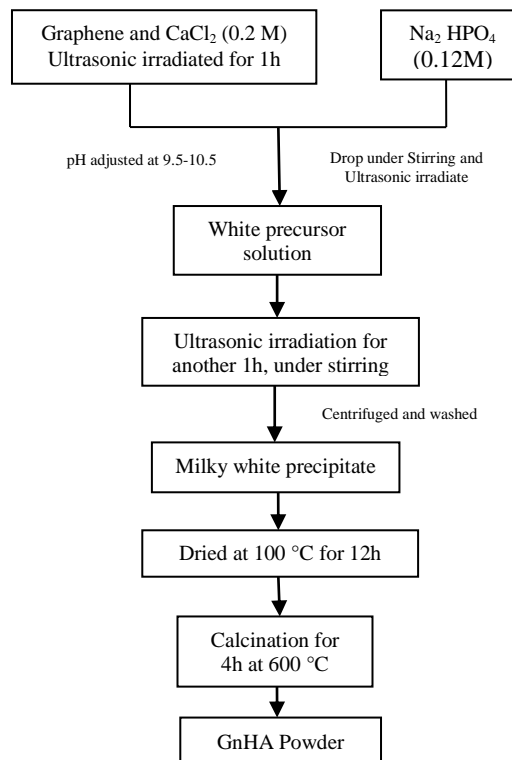

Figure 1 Flow chart for the synthesis of Graphene/nanohydroxyapatite composite by ultrasonic assisted method.

SEM characterization was carried out using a QUANTA FEG 250 type instruments in vacuum environment. Prior to analysis samples composites were sprinkled onto Al or C tapes which are adhesive and supported on metallic disks and coated with Au. Images of the sample surfaces were recorded at different areas and magnifications. In this work, Bruker optics VERTEX 7000 Fourier Transform Infrared Spectrometer was used for recording the IR spectra. Spectra were recorded in a spectral range of 4000–400 cm^{-1}, resolution 2 cm^{-1} and scan speed 2mm/sec. The obtained spectrum was automatically recorded on a computer whose scales in transmittance/ Absorbance against wave number (cm^{-1}). The thermal decomposition behavior and required sintering temperature of citrate precursor to phase formation of the sample was checked by Thermogravimetric analysis on the SDT Q-600 instrument by heating the powder after auto-

combustion in air atmosphere from 20 to 1000 °C at the rate of 10 °C per min. Dynamic light scattering (DLS) results were recorded by a Malvern zetasizer, United Kingdom. The mechanical testing was running for the sintered composite pellets using a Universal Instron Mechanical Testing System (Instron 5982). All the mechanical testing was running under room temperature, at 0.5mm/min crosshead speed. The compressive strength was calculated from the maximum load registered during the test divided by the original area. Each measurement was repeated replicates, and then the averages of the compressive strength values were taken.

3. Results and Discussion

It is well known that the growth pattern and nucleation are highly affecting the homogeny of particle size during the preparation process, it found to be greatest in the liquid phase due to the supersaturation degree achievement. When ultrasonic irradiation using in the preparation process produced micro jets and shock waves through the collapsing of microbubbles which generates hot spots with fast cooling rates [25], accordingly these phenomena can initiate chemical reactions and physical alteration, accordingly ultrasound irradiation can be used in the synthesis process of materials in the liquid phase.

The cavitations in the liquid can be affected by the ultrasonic irradiation power, a huge cavitations number will be produced during using high sonication power through the generation of more transient bubbles. As a result of using ultrasonic irradiation, more nucleation sites are produced the particles formed around these sites are expected to be smaller for the same original reagent concentration. Moreover, the particles get for contacts for longtime with ultrasonic waves are expected to exhibit minimum agglomeration level. HR-SEM results showed well dispersion samples as an using of ultrasonic irradiation in the preparation process.[14]

Generally in aqua solution Ca^{2+} and P^{-3} ions are mixing through the diffusion of the ions from higher to lower concentrations. Consequently, by elevated the pH value to around 10, a white precipitate is formed immediately, then by washing using water and ethanol the excess of chemicals can be removed. After that, the collected precipitate is calcined at a high temperature. The obtained nanoparticles exhibited a high degree of disturbance in their particle size due to agglomeration. Therefore, ultrasonic irradiation can be used during the precipitation reaction in order to achieve the uniform shape and size distribution of the nHA nanoparticles. Ultrasonic irradiation affects the cavitation process in which small bubbles or cavities are formed and as a result of ultrasonic irradiation, huge thermal energies are producing inside those cavities which leading to the collapse of these cavities. The formation of cavitation which is followed by cavitation collapse is finally leading to the production of a uniform particle size distribution of the nanoparticles trapped in these cavities.[26]

3.1. SEM and TEM microscopy analysis.

Transmission electron microscopy (TEM) provided very useful information about shape and size of the particle of both the nanocrystalline Hydroxyapatite (nHA) and Graphene nanocrystalline Hydroxyapatite (G2nHA) powders. A typical TEM micrograph of the nHA ultrafine powder is presented in Figure 2 (a, b) and complete surface morphology of the cylindrical particles has been revealed, which is similar to the particle morphologies reported in the literature [27]. The particle size of nHA determined from TEM images was found to be about 70 nm for HA and about 50 nm. Fig.2 (c, d, f) show the TEM images of G2nHA and explore the existing of graphene sheets and the growth of nHA on it and well dispersed without evident aggregation. The images suggest that the particles size of around 75 nm and this value is in the close vicinity to value obtained from XRD analysis. There is additional shown obtained from TEM micrographs that the even a single particle is consist of small crystallites which is clearly seen in Figure 2 (a, d and f) for both nHA and G2nHAwhere lattice images of many crystallites that form the particle are shown clearly and independently. The size of these crystallites for G2nHA as shown in Figure.2 (f) is about 0.3 nm. This observation was also found to be in good agreement with results obtained from XRD calculations small crystallites which are seen in Figure 2 (a, d, and f).

Figure 3(a, b) exhibited the SEM micrographs which have been invoked to provide the morphology

of the obtained nHA and G2nHA samples. Figure 3(a, b) shows the SEM images of nHA particles and reveals that as prepared samples consist of pure hydroxyapatite having rod-like shape with separated with infinitesimal distance.
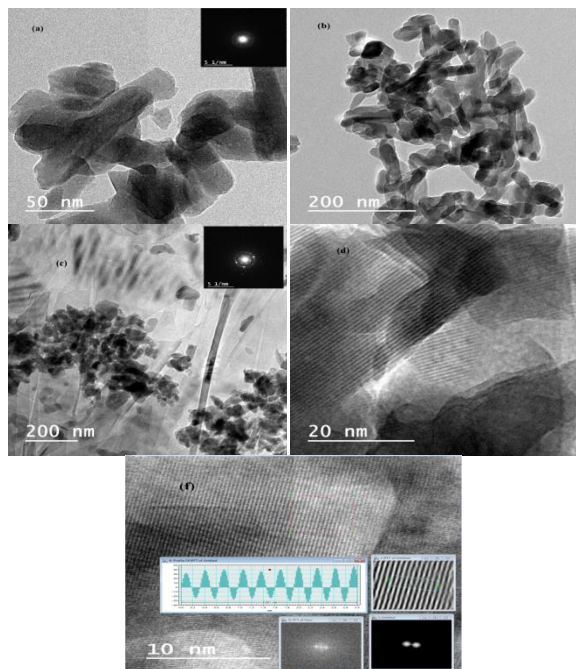

Figure 2 TEM of nHA (a and b) and G2nHA(c, d and f).

3.2. Energy dispersive X-ray spectroscopy (EDAX) analysis.

This technique was used to analyze the nHA and G2nHA samples and its elemental structure. Composition of elementals and particles homogeneity has significant and detectable effects on the biocompatibility and the bioactivity properties of such material. The EDAX spectra of nHA and G2nHA samples are shown in Figure 3 (c, d). EDAX result reveals that the samples contain Ca, P and O without any impurity (except from small traces of C for G2nHA sample due to the graphene presence). The Ca/P ratio calculation from the EDAX spectra gives a value of 1.66 and 1.73 for nHA and G2nHA samples which is matched with the stoichiometric value 1.67 (theoretical value) used in the ultrasonic process to create HA and the same was commonly reported [28]. The close agreement of the Ca/P not only indicates the successful preparation of nHA, but also confirms that the production of high-quality nHA powders. The (EDAX) analysis is confirmed with the results of the XRD analysis.
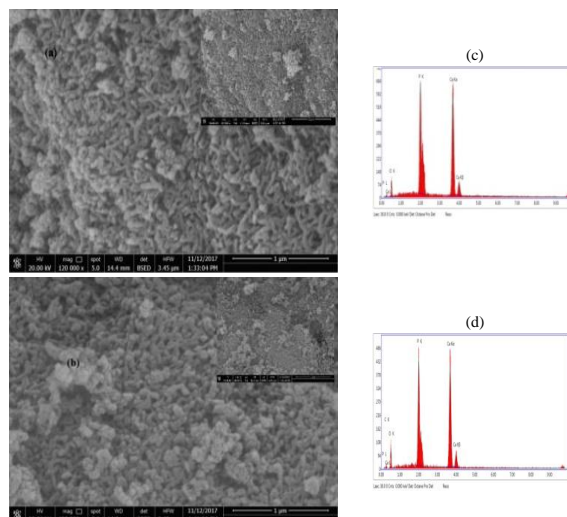

Figure 3 SEM micrographs of (a) nHA and (b) G2nHA. EDAX spectra show elemental presence of (c) nHA and (d) G2nHA. Where, C (carbon), Ca (calcium), P (phosphorous) and O (oxygen).

3.3. XRD patterns and phase formation

Figure 4 presents the XRD patterns of hydroxyapatite nanocrystalline (nHA) and that doped with graphene (G1nHA, G2nHA and G3nHA), calcined at 600ºC. The XRD spectrum of nHA nanocrytalline sample shows feature distinct peaks at 2θ = 22.91°, 25.89°, 28.13°, 28.94°, 31.75°, 32.15°, 32.89°, 34.03°, 39.75°, 41.88°, 46.69°, 48.09°, 49.51°, 50.5°, 51.27°, 52.08°, 53.2°, 62.99°, and 63.9°, which were indexed to the (111), (002), (012), (120), (121), (112), (030), (022), (130), (131), (222), (132), (123), (231), (140), (042), (004), (052), and (034) planes of Hydroxyapatite (Calcium Phosphate Hydroxide $Ca_{10}(PO_4)_6(OH)_2$, respectively, in accordance with the standard data for hexagonal $Ca_{10}(PO_4)_6(OH)_2$ (JCPDS No. 00-064-0738). Additionally, the GnHA phase almost shows the same behavior of nHA, and there is emerging of new peak for GnHA samples (G1nHA, G2nHA and G3nHA) at about 26.65° which attributed to the crystalline phase of graphene [29,30]. Furthermore, the presents of graphene demonstrates an improvement in the shape and intensity of the peaks with highly pitched diffraction peaks signifying the establishment of good crystalline structure.
The average crystallite size was determined for calcined powder from broadening of XRD peaks using Scherrer equation

$$D = \frac{K\lambda}{\beta \cos\theta}$$

Where K is the shape factor (around 0.9), θ=Bragg's angle (2θ = 32.15°), λ=X-ray wavelength (1.54 0A), and B=FWHM [31]. The mean crystallite size (D) for nHA, G1nHA, G2nHA and G3nHA was 28.2nm, 64.9nm, 67.4nm and 69.2 nm respectively.
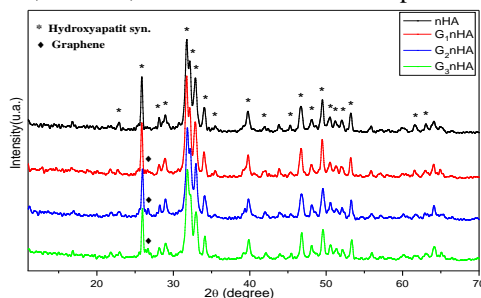

Figure 4. XRD patterns of nHA and Graphene nHA samples (G1nHA, G2nHA and G3nHA).

3.4. FTIR analysis.

Figure 5 exhibits representative FT-IR spectra of four HA nanoparticles samples synthesized under in-situ ultrasonic method. Approximately all spectra have similar band location and intensities normally associated with nanoscale HA.

Careful examination of Figure 5 show that the band located at 962 cm^{-1} is associated with ν1 symmetric stretching vibrations normally associated with the P-O mode. The very strong bands presented at 1025 cm^{-1} and 1089 cm^{-1} revealed the presence of PO_4 functional groups (P-O mode)[32]. The weak band for phosphate bending vibration appears at 472 cm^{-1}. Moreover, the doublet band at 562-600 cm^{-1} was assigned to the PO_4 bending mode. The small peak located approximately at 3500 cm^{-1} and 632 cm^{-1} corresponds to stretching mode and vibrational mode of the OH− group [33]. A small band at around 1650 cm^{-1} was possibly due to absorbed water. While the weak peak at 3575 cm^{-1} corresponds to the stretching vibration of OH^{-1} ions in the HA lattice [14,34]. This indicates that the samples are of high quality and found to be very similar to those observed in the literature [28,35,36]

Raman spectroscopy was carried out in order to detect the fundamental vibrational bands in the hydroxyapatite lattice as it presented in figure 5b. The Raman spectrum of pure nHA showed remarkable four essential vibration modes of the PO_4

unit in the hydroxyapatite structure appear at 431 cm^{-1}, 591 cm^{-1}, 960 cm^{-1}, 1038 cm^{-1}, and 3568 cm^{-1} which mainly are assigned to symmetric bending mode v2, antisymmetric bending mode v4, symmetric stretching mode v1 and antisymmetric stretching mode v3 respectively. Raman spectra for Graphene/nHA composites showed additional two vibrational bands namely D mode ≈1340 cm^{-1} and G mode ≈1575 cm^{-1} which are characteristic band for graphene sheet like structure and the intensities of those bands are increasing by rising up the graphene loading percentage in the composites. The presence of those two band in Raman spectra gives strong evidence of the incorporation of graphene sheets into the hydroxyapatite structure.
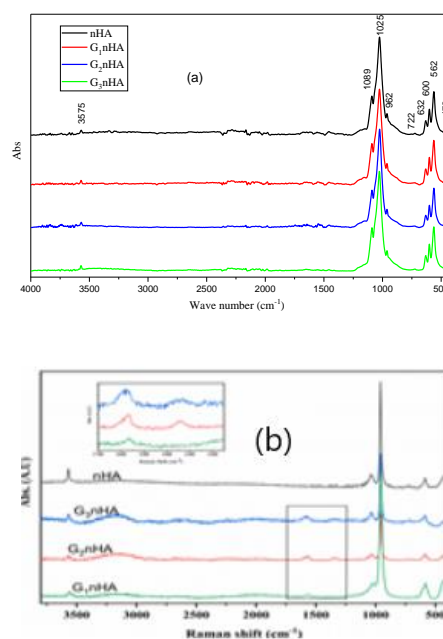

Figure 5 FT-IR spectra (a) and Raman spectra (b) of nHA and Graphene-nHA with different concentration G1nHA, G2nHA and G3nHA.

3.5. Zeta potential analysis.

The Zeta potential of the nHA and Graphene-nHA with different concentration G1nHA, G2nHA, and G3nHA colloidal dispersion was measured at pH = 7 and expressed in Figure 6. The Zeta potential was -18.06 mV, -16.41, -17.39 mV and -21.31mV mV for nHA, G1nHA, G2nHA, and G3nHA respectively. the Zeta potential value of nHA is very close to the stoichiometric value that reported for pure HA (

−18.1 mV)[37]. The gradual increase of negative values of zeta potential indicates the size increase which could be attributed to agglomeration of graphene sheet like structure by increasing the loading percentage of graphene and these results are consistence with the previous study reported by Chen et al [38].
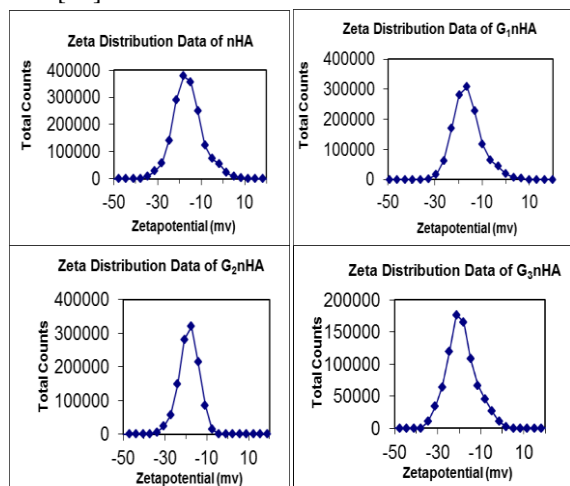

Figure 6 Zeta potential analyses of nHA and GnHA samples.

3.6. TGA analysis.

Thermal stability of GnHA samples was examined by thermal decomposition of the nanopowders. The TGA and DTA curves as shown in Figure 7 presented the thermal decomposition of nHA and GnHA samples (G2nHA and G3nHA). It was observed that decomposition of HA sample below 200 °C due to removal of absorbed water. Approximately, there is an un-measurable weight loss detected from 200 to 770°C. Then the weight loss of about 2% from 770 to 920°C, which is possibly by means of slow exclusion of carbonate groups linked to HA [39]. Which can confirm by FTIR results previously discussed? There is no measureable decomposition detected between 920∘C to 1100∘C, which proves the thermal stability of prepared nHA up to 1100∘C [26]. DTA curve shows that thermal decomposition of HAP sample at 100 °C, and 780 °C with an endothermic peak and this peak is only due to degradation of residual water and from slow elimination of carbonate groups linked to HA.
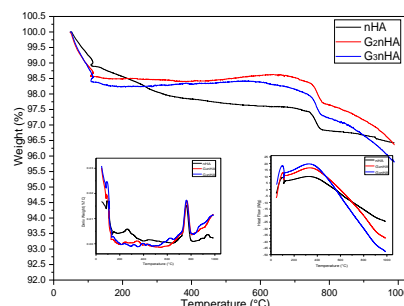

Figure 7. TGA and DTA curves of nHA and GnHA samples (G2nHA and G3nHA).

3.7. Mechanical testing analysis of nHA and G-nHA composites.

The maximum compressive strength values of the calcined pure nHA and Graphene nHA composites are measured in order to evaluate the mechanical behavior, the mean value of the three replicates is shown in Figure 8. The value of compressive strength for pure nHA is 85.79 ± 4 MPa, which point to that pure nHA can't be used as a high-strength material for load-bearing applications. The compressive strength value is dramatically enhanced with adding of graphene sheets like structure which reinforcement up to 128.9 ± 7 MPa. The compressive strength values for G–nHA composites (1, 2, 3% wt. G in nHA) were sharp increases in case of G1nHA (128.9 ± 7) then decreased gradually by increasing the Graphene loading percentage (G2nHA, G3nHA) 121.7 ± 6 MPa and 103.34 ± 5 MPa respectively. These reinforcement might be attributed to the wrapping performance of Graphene sheets like structure around nHA particles which enhancement the mechanical interconnecting and minimized the shrinkage within the nHA matrix. Even though the maximum mechanical force enhancement was found for G1nHA samples (1% of Graphene loading). The decline in the increase of compressive strength could attribute to the defects or aggregation of Graphene sheets created through the preparation process. Considering the Graphene amount and compressive strength values for G1nHA (1%) composite displayed the optimum mechanical performance when compared to the other composites and this finding are very close to the previous work by other researcher [40].
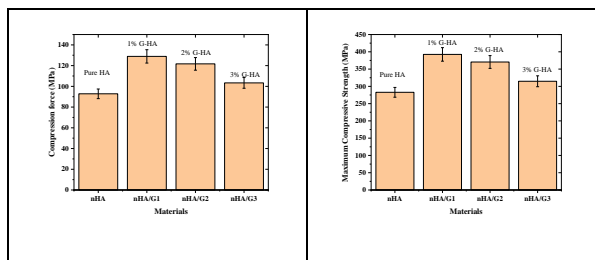
Figure 8 Compression force and Maximum compression strength
for nHA, G1nHA, G2nHA and G3nHA

Conclusions

The study has shown that ultrasonic irradiation played an important role in determining crystallite size, particle size and particle morphology. In this study it is reported that HA nanopowders were produced using the straightforward wet chemical method using Sodium phosphate dibasic and calcium chloride as precursors. Furthermore the employing of ultrasonic irradiation through preparation process resulting in formation of HA powders in the nano-range with a reasonably particle size distribution, which is predominantly cylindrical and granular ranging in size from 70 nm for HA and about 50 nm for G2nHA. Additionally, as it shown from TEM images, the using of graphene resulted in the decrease of the nHA particle size. The Ca/P ratio calculation from the EDAX spectra gives a value of 1.66 and 1.73 for nHA and G2nHA samples which is very close to the stoichiometric value 1.67 (theoretical value) used in the ultrasonic process to create HA. The close agreement of the Ca/P not only reveals the presence of nHA, but also confirms that the produced nHA powders are of high quality. FTIR spectra and XRD patterns identifying the samples as nanoscale HA and reveals that the prepared powders are hydroxyapatite (Calcium Phosphate Hydroxide $Ca_{10}(PO_4)6(OH)_2$), in accordance with the standard data for hexagonal $Ca_{10}(PO_4)6(OH)2$.

The composites were mechanically evaluated to understand the mechanical effects of Graphene incorporation in the nHA structure. The prepared composites displayed that even a small amount of graphene can reinforcement significantly the compressive strength of the HA sample. The optimum increase was observed for the RGO–HA 1% composite.

References

[1]   M. Vallet-Regí, J.M. González-Calbet, Calcium phosphates as substitution of bone tissues, Prog. Solid State Chem. (2004). https://doi.org/10.1016/j.progsolidstchem.2004.07.001.

[2]   S. V. Dorozhkin, Nanodimensional and nanocrystalline apatites and other calcium orthophosphates in biomedical engineering, biology and medicine, Materials (Basel). (2009). https://doi.org/10.3390/ma2041975.

[3]   Y. Cai, R. Tang, Calcium phosphate nanoparticles in biomineralization and biomaterials, J. Mater. Chem. (2008). https://doi.org/10.1039/b805407j.

[4]   AOKI, H, Science and medical applications of hydroxyapatite, JAAS. 1991 (n.d.) 123–134.

[5]   LEGEROS, RZ, Calcium phosphates in oral biology and medicine, Monogr. Oral Sci. 15 (1991) 109–111.

[6]   A. Blom, (V) Which scaffold for which application?, Curr. Orthop. (2007). https://doi.org/10.1016/j.cuor.2007.06.005.

[7]   P. Habibovic, K. de Groot, Osteoinductive biomaterials - properties and relevance in bone repair, J. Tissue Eng. Regen. Med. (2007). https://doi.org/10.1002/term.5.

[8]   M. Taniguchi, H. Takeyama, I. Mizuno, N. Shinagawa, J. Yura, N. Yoshiyama, H. Aoki, The clinical application of intravenous catheter with percutaneous device made of sintered hydroxyapatite, Japanese J. Artif. Organs. (1991). https://doi.org/10.11392/jsao1972.20.460.

[9]   R. V. Silva, J.A. Camilli, C.A. Bertran, N.H. Moreira, The use of hydroxyapatite and autogenous cancellous bone grafts to repair bone defects in rats, Int. J. Oral Maxillofac. Surg. (2005). https://doi.org/10.1016/j.ijom.2004.06.005.

[10]   A.M. El Nahrawy, B.A. Hemdan, A.B. Abou Hammad, A.L.K. Abia, A.M. Bakr, Microstructure and Antimicrobial Properties of Bioactive Cobalt Co-Doped Copper Aluminosilicate Nanocrystallines, Silicon. (2020). https://doi.org/10.1007/s12633-019-00326-y.

[11]   A.M.E. Nahrawy, A.M. Bakr, A.B.A. Hammad, B.A. Hemdan, High performance of talented copper/magneso-zinc titanate nanostructures as biocidal agents for inactivation of pathogens during wastewater disinfection, Appl. Nanosci. (2020). https://doi.org/10.1007/s13204-020-01454-3.

[12] A.A. Al-esnawy, K.T. Ereiba, A.M. Bakr, A.S. Abdraboh, Characterization and antibacterial activity of Streptomycin Sulfate loaded Bioglass/Chitosan beads for bone tissue engineering, J. Mol. Struct. (2021). https://doi.org/10.1016/j.molstruc.2020.129715.

[13] K.S. Vecchio, X. Zhang, J.B. Massie, M. Wang, C.W. Kim, Conversion of bulk seashells to biocompatible hydroxyapatite for bone implants, Acta Biomater. (2007). https://doi.org/10.1016/j.actbio.2007.06.003.

[14] G.E. Poinern, R.K. Brundavanam, N. Mondinos, Z.T. Jiang, Synthesis and characterisation of nanohydroxyapatite using an ultrasound assisted method, Ultrason. Sonochem. (2009). https://doi.org/10.1016/j.ultsonch.2009.01.007.

[15] B. Nasiri-Tabrizi, P. Honarmandi, R. Ebrahimi-Kahrizsangi, P. Honarmandi, Synthesis of nanosize single-crystal hydroxyapatite via mechanochemical method, Mater. Lett. (2009). https://doi.org/10.1016/j.matlet.2008.11.030.

[16] S.K. Padmanabhan, A. Balakrishnan, M.C. Chu, Y.J. Lee, T.N. Kim, S.J. Cho, Sol-gel synthesis and characterization of hydroxyapatite nanorods, Particuology. (2009). https://doi.org/10.1016/j.partic.2009.06.008.

[17] G.C. Koumoulidis, A.P. Katsoulidis, A.K. Ladavos, P.J. Pomonis, C.C. Trapalis, A.T. Sdoukos, T.C. Vaimakis, Preparation of hydroxyapatite via microemulsion route, J. Colloid Interface Sci. (2003). https://doi.org/10.1016/S0021-9797(02)00233-3.

[18] A.J. Salgado, O.P. Coutinho, R.L. Reis, Bone tissue engineering: State of the art and future trends, Macromol. Biosci. (2004). https://doi.org/10.1002/mabi.200400026.

[19] S. Brundavanam, G.E.J. Poinern, D. Fawcett, Synthesis of a Hydroxyapatite Nanopowder via Ultrasound Irradiation from Calcium Hydroxide Powders for Potential Biomedical Applications, Nanosci. Nanoeng. (2015). https://doi.org/10.13189/nn.2015.030101.

[20] W. El hotaby, A.M. Bakr, H.S. Ibrahim, N.S. Ammar, H.A. Hani, A.A. Mostafa, Eco-friendly zeolite/alginate microspheres for Ni ions removal from aqueous solution: Kinetic and isotherm study, J. Mol. Struct. 1241 (2021) 130605. https://doi.org/10.1016/j.molstruc.2021.130605.

[21] A.M. El Nahrawy, A.B. Abou Hammad, A.M. bakr, T.I. Shaheen, A.M. Mansour, Sol–gel synthesis and physical characterization of high impact polystyrene nanocomposites based on Fe2O3 doped with ZnO, Appl. Phys. A Mater. Sci. Process. 126 (2020) 1–11. https://doi.org/10.1007/s00339-020-03822-w.

[22] amany el nahrawy, ahmed bakr, A. abou hammad, A.-F. Mansour, Nano-architecture of CaO/Ag-chitosan nanocomposite by sol gel process: formation and characterization, Egypt. J. Chem. 0 (2021) 0–0. https://doi.org/10.21608/ejchem.2021.80608.3995.

[23] M. Eilbagi, R. Emadi, K. Raeissi, M. Kharaziha, A. Valiani, Mechanical and cytotoxicity evaluation of nanostructured hydroxyapatite-bredigite scaffolds for bone regeneration, Mater. Sci. Eng. C. (2016). https://doi.org/10.1016/j.msec.2016.06.030.

[24] M.A. Moharram, K.M.T. Ereiba, W. El Hotaby, A.M. Bakr, Synthesis and characterization of graphene oxide/crosslinked chitosan nanaocomposite for lead removal form aqueous solution, Res. J. Pharm. Biol. Chem. Sci. 6 (2015) 1473–1489.

[25] L. Guardia, M.J. Fernández-Merino, J.I. Paredes, P. Solís-Fernández, S. Villar-Rodil, A. Martínez-Alonso, J.M.D. Tascón, High-throughput production of pristine graphene in an aqueous dispersion assisted by non-ionic surfactants, Carbon N. Y. (2011). https://doi.org/10.1016/j.carbon.2010.12.049.

[26] D. Gopi, J. Indira, L. Kavitha, M. Sekar, U.K. Mudali, Synthesis of hydroxyapatite nanoparticles by a novel ultrasonic assisted with mixed hollow sphere template method, Spectrochim. Acta - Part A Mol. Biomol. Spectrosc. (2012). https://doi.org/10.1016/j.saa.2012.02.033.

[27] F.C. Oliveira, J.O. Carvalho, S.B.S. Gusmão, L. de S. Gonçalves, L.M.S. Mendes, S.A.P. Freitas, G.O. de M. Gusmão, B.C. Viana, F.R. Marciano, A.O. Lobo, High loads of nano-hydroxyapatite/graphene nanoribbon composites guided bone regeneration using an osteoporotic animal model, Int. J. Nanomedicine. (2019). https://doi.org/10.2147/IJN.S192456.

[28] P.N. Jagadale, P.P. Jagtap, M.G. Joshi, S.R. Bamane, A prototype synthesis and characterization of hydroxyapatite bioceramics nanocrystallites, Adv. Mater. Lett. (2016). https://doi.org/10.5185/amlett.2016.5837.

[29] W.A. Khalil, H.H.A. Sherif, B.A. Hemdan,

_____

S.K.H. Khalil, W. El Hotaby, Biocompatibility enhancement of graphene oxide-silver nanocomposite by functionalisation with polyvinylpyrrolidone, IET Nanobiotechnology. (2019). https://doi.org/10.1049/iet-nbt.2018.5321.

[30] B. Anis, A. Abouelsayed, W. El hotaby, A.M. Sawy, A.S.G. Khalil, Tuning the plasmon resonance and work function of laser-scribed chemically doped graphene, Carbon N. Y. (2017). https://doi.org/10.1016/j.carbon.2017.05.010.

[31] E. Atkins, Elements of X-ray Diffraction, Phys. Bull. (1978). https://doi.org/10.1088/0031-9112/29/12/034.

[32] G.W. Ali, W. El-Hotaby, B. Hemdan, W.I. Abdel-Fattah, Thermosensitive chitosan/phosphate hydrogel-composites fortified with Ag versus Ag@Pd for biomedical applications, Life Sci. (2018). https://doi.org/10.1016/j.lfs.2017.12.021.

[33] S.K.H. Khalil, W.M. El Hotaby, G.T. El-Bassyouni, Terahertz pulsed spectroscopy for optical and dielectric properties of demineralized bone matrix, collagen and hydroxyapatite, Egypt. J. Chem. (2019). https://doi.org/10.21608/EJCHEM.2019.14201.1876.

[34] M. Mujahid, S. Sarfraz, S. Amin, On the formation of hydroxyapatite nano crystals prepared using cationic surfactant, Mater. Res. (2015). https://doi.org/10.1590/1516-1439.298014.

[35] D. Gopi, S. Nithiya, E. Shinyjoy, L. Kavitha, Spectroscopic investigation on formation and growth of mineralized nanohydroxyapatite for bone tissue engineering applications, Spectrochim. Acta - Part A Mol. Biomol. Spectrosc. (2012). https://doi.org/10.1016/j.saa.2012.02.069.

[36] V. Stanić, D. Janaćković, S. Dimitrijević, S.B. Tanasković, M. Mitrić, M.S. Pavlović, A. Krstić, D. Jovanović, S. Raičević, Synthesis of antimicrobial monophase silver-doped hydroxyapatite nanopowders for bone tissue engineering, Appl. Surf. Sci. (2011). https://doi.org/10.1016/j.apsusc.2010.12.113.

[37] Y. Wang, S. Zhang, K. Wei, N. Zhao, J. Chen, X. Wang, Hydrothermal synthesis of hydroxyapatite nanopowders using cationic surfactant as a template, Mater. Lett. (2006). https://doi.org/10.1016/j.matlet.2005.11.053.

[38] L. Chen, J.M. Mccrate, J.C.M. Lee, H. Li, The role of surface charge on the uptake and biocompatibility of hydroxyapatite nanoparticles with osteoblast cells,

Nanotechnology. (2011). https://doi.org/10.1088/0957-4484/22/10/105708.

[39] P.N. Kumta, C. Sfeir, D.H. Lee, D. Olton, D. Choi, Nanostructured calcium phosphates for biomedical applications: Novel synthesis and characterization, Acta Biomater. (2005). https://doi.org/10.1016/j.actbio.2004.09.008.

[40] Ö. Elif, Ö. Belma, Ş. Ilkay, Production of biologically safe and mechanically improved reduced graphene oxide/hydroxyapatite composites, Mater. Res. Express. (2017). https://doi.org/10.1088/2053-1591/aa5464.

_____